CHALMERS
UNIVERSITY OF TECHNOLOGY

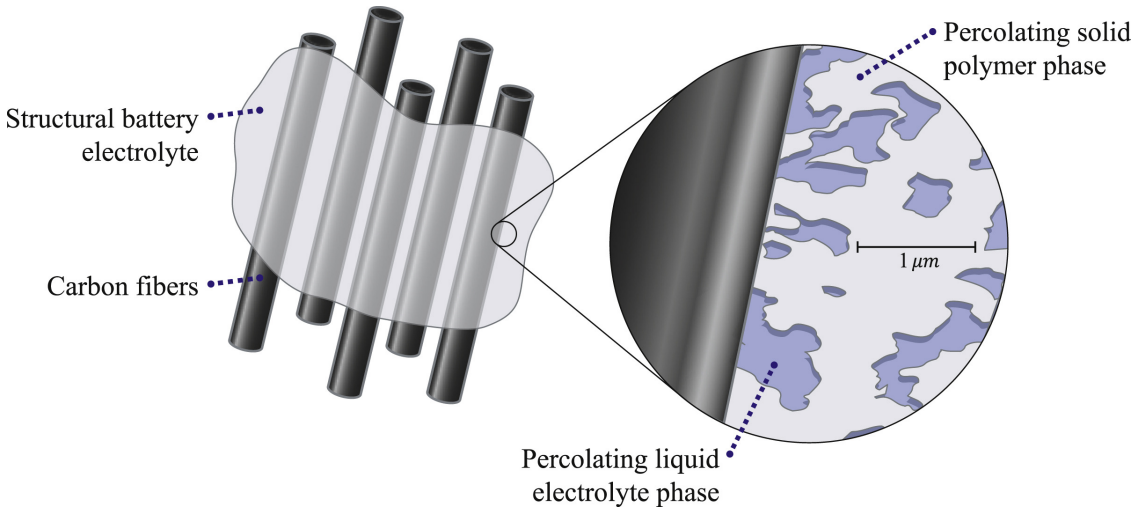

Simulation of deformation in a porous structural battery electrolyte:

The effect on the electrochemical properties

Master's thesis in Applied Mechanics

KONSTANTINOS PSYRIDIS

Department of Industrial and Materials Science
CHALMERS UNIVERSITY OF TECHNOLOGY
Gothenburg, Sweden 2020

Master's thesis 2020

Simulation of deformation in a porous structural battery electrolyte: The effect on the electrochemical properties

KONSTANTINOS PSYRIDIS

CHALMERS
UNIVERSITY OF TECHNOLOGY

Department of Industrial and Materials Science
Division of Material and Computational Mechanics
Chalmers University of Technology
Gothenburg, Sweden 2020

Simulation of deformation in a porous structural battery electrolyte:
The effect on the electrochemical properties
KONSTANTINOS PSYRIDIS

Supervisor: Dr. Johanna Xu, Chalmers University of Technology, Department of Industrial and Materials Science
Examiner: Prof. Leif Asp, Chalmers University of Technology, Department of Industrial and Materials Science

Master's Thesis 2020
Chalmers University of Technology
Department of Industrial and Materials Science
Chalmers University of Technology
SE-412 96 Gothenburg
Telephone +46 31 772 1000

Cover: Cover page illustration from Xu et. al. Compos. Sci. Technol., 2020. [1]

Typeset in LaTeX
Printed by Chalmers Reproservice
Gothenburg, Sweden 2020

Simulation of deformation in a porous structural battery electrolyte:
The effect on the electrochemical properties
KONSTANTINOS PSYRIDIS
Department of Industrial and Materials Science
Chalmers University of Technology

Abstract

There is a great demand nowadays for a sustainable environment. Structural batteries are an innovative solution which can bear mechanical and electrical loads at the same time. They are multifunctional materials capable to provide electric energy and mechanical support. Integration of structural batteries in the transportation section will be beneficiary leading to a more carbon neutral economy.
Two structural battery architectures have been proposed. A laminated half cell setup was implemented in the current analysis. The structure consists of two electrodes, the separator and the structural battery electrolyte (SBE). Lithium metal and carbon fibre (CF) were used as negative and positive electrode respectively. The SBE is a microporous polymer matrix, which consists of solid polymer network and liquid electrolyte trapped in the cavities. This microstructure is responsible for the multifunctional performance of the SBE which allow lithium ions to transport through the liquid phase whereas the solid area provide mechanical support.
One cycle of lithiation was computed in the current thesis work. During lithiation, lithium ions intercalate in the microstructure of the carbon fibre leading to the fibre's expansion. This swelling compresses the surrounded SBE and affects its properties. Pores are closing due to the compression and the ion conductivity is decreasing over time. In order to model the response of the SBE and CF linear elasticity is used. Also, linear relation between porosity and volumetric strains, which occurred in the SBE, domain was implemented.
The results indicate that there is a strong relation between porosity and ion conductivity. Further, experimental work is necessary for validation of the simulations.

Keywords: strucural battery electrolyte, carbon fibre, electrode, intercalation, lithiation, swelling, ion conductivity

Acknowledgements

This project is the final piece towards the end of the master's programme in Applied Mechanics at Chalmers University of Technology. It was conducted during the spring semester 2020. It allowed me to discover my passion for research and collaborate with amazing people each of whom I would like to thank separately.
First and foremost, I would like to express my special thanks of gratitude to my supervisor Dr. Johanna Xu for her guidance, support and motivation throughout this period.
A special mention goes to David Carlstedt, who helped with his support and knowledge on the topic during the meetings.
Also, I would like to extend my gratitude to my examiner Prof. Leif Asp for engaging actively in the discussions. Invaluable was my participation on TRACKS project coordinated by Leif Asp, which helped me understand the concept of structural batteries even better.
Finally, a special thank you to my family and my sister for the support during this stressful period of time.

Konstantinos Psyridis, Gothenburg, June 2020

Contents

List of Figures

1

Introduction

1.1 Background

There is a growing worldwide demand for decreasing the environmental footprint. This can be succeeded by using electric energy from renewable resources instead of fossil fuels, leading towards a more sustainable and carbon-neutral circular economy. Electrification has already been introduced, with the usage of batteries on many applications especially in the transport sector. The integration of batteries in vehicles raised a significant challenge; that is the additional weight. This is inevitable in order for the vehicle to have sufficient driving range. However, the large and heavy battery pack limits the range and does not contribute to the integrity of the vehicle in case of an accident. For this reason, novel architectures with multifunctional properties are under investigation. Lightweight composite materials that can bear mechanical and electrical loads at the same time, referred as structural batteries, have been shown as a way to decrease the mass of the vehicles [2, 3, 4, 5]. Multifunctional materials differ from multifunctional structures. The former refers to materials which can have more than one functionality, e.g. carbon fibres intercalate lithium ions and act as mechanical reinforcement. The latter, refers to systems that are assembled by many materials with different properties and each one of these provide its own functionality. The first attempts to manufacture this structure from multifunctional constituents were performed by the US Army Research Labs [6, 7].

1.2 Structural Batteries

The structural battery is a composite material made of carbon fibre reinforced polymer (CFRP). Until these days carbon fibres are widely used because of their good mechanical properties, such as high strength and stiffness to weight ratio. However, studies have shown they also have good electrochemical properties, due to their ability to intercalate lithium ions in a similar way as a negative graphite electrode in commercial lithium ion batteries [8]. Intercalation is the process where lithium cations (Li^+, positively charged lithium due to the loss of the electron) are accommodated in the crystal lattice of the host material, which in the current analysis is the carbon fibre. A schematic of lithium ions intercalation process is depicted in Figure 1.1.

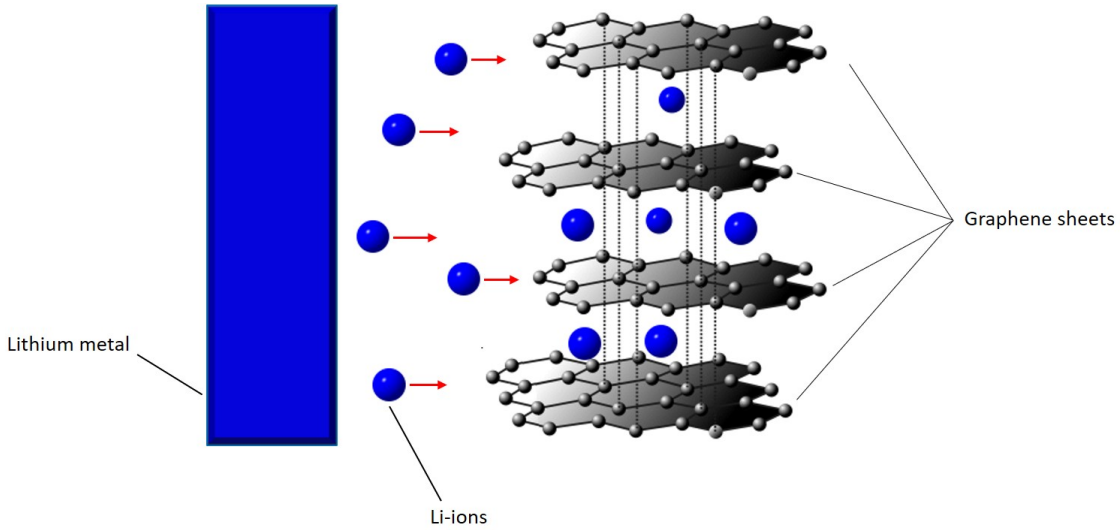

Figure 1.1: Schematic of lithium ions intercalation in graphene crystal lattice.

In such a battery structure, carbon fibres act as reinforcement and electrode whereas the polymer functions as matrix and electrolyte. The electrolyte is a medium that allows the ions (positive or negative charged particles) to travel between the electrodes, during lithiation and delithiation. The ions are transported through the electrolyte and electrons flow in an external circuit and that is what generate electric current. Such a novel architecture is depicted in Figure 1.2.

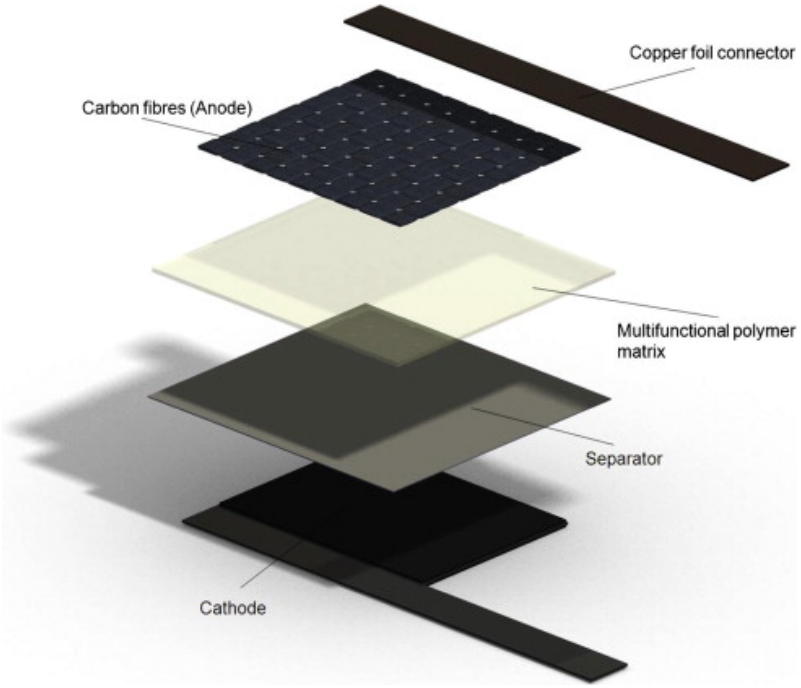

Figure 1.2: Architecture of a laminate structural battery [9].

Two types of structural batteries have been proposed; a) a laminated battery cell presented by Wetzel et al. [10] and demonstrated by Ekstedt et al. [11] and Carlson [12] and b) a 3D battery presented by Asp and co-workers [9, 13]. Schematic versions of these architectures are illustrated in Figure 1.3

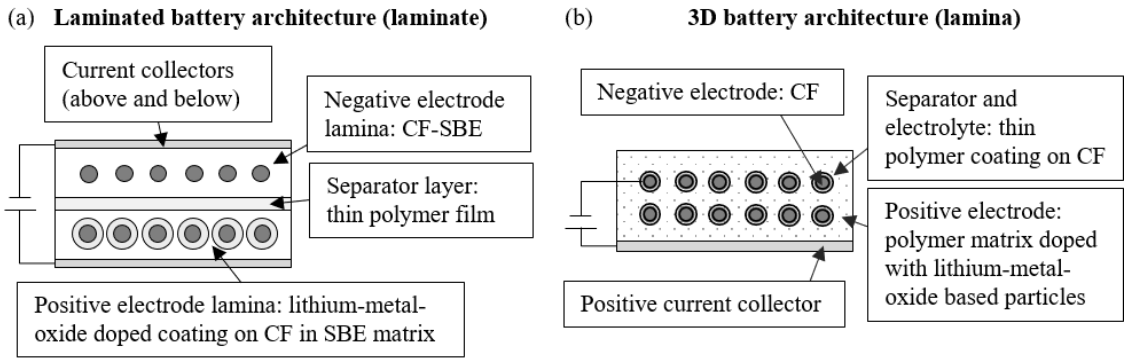

Figure 1.3: Schematic illustration of the different approaches of the structural batteries (CF=carbon fibre, SBE=structural battery electrolyte). a) laminated battery b) 3D battery [14].

The former architecture consists of laminae which have different functionalities. The negative electrode consists of carbon fibres, which are surrounded by a heterogeneous polymers electrolyte, referred as structural battery electrolyte (SBE), introduced by Ihrner et al. [15]. This polymer electrolyte is of great importance. Commercial lithium ion batteries use liquid electrolyte which is unable to provide mechanical support in a structure. For this reason, research is being conducted, and heterogeneous structures are proposed [16]. Those systems are called heterogeneous or bi-continuous, because two continuous phases (solid and liquid) exist simultaneously, as Figure 1.4 depicts. Further information regarding these structures is presented in subsection 1.2.1.

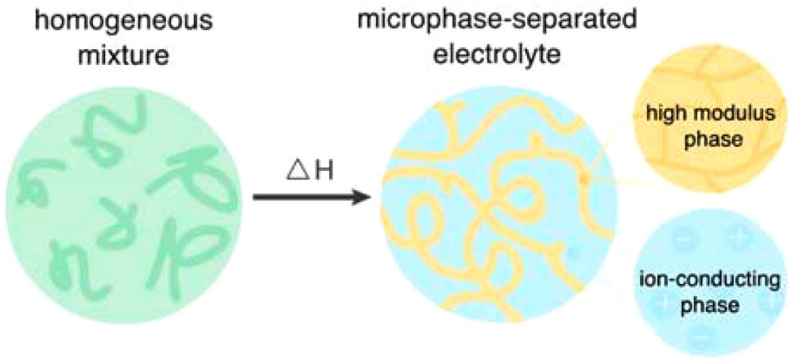

Figure 1.4: Schematic approach of bi-continuous material [16].

The positive electrode consists of SBE which is reinforced with lithium-based electrode material coated carbon fibre, such as $LiFePO_4$. Finally, the electrodes are separated by a separator layer which prevents the battery from short-circuit.

The 3D battery consists of individual carbon fibres which act as negative electrodes and are coated with a thin film of polymer electrolyte. The coated fibres are doped into the polymer matrix which contains lithium metal oxide particles or phosphate and acts as the positive electrode.

1.2.1 Structural battery electrolyte

The structural battery electrolyte (SBE) has two different purposes. It allows lithium ions to be transported and it transfers mechanical loads between the carbon fibres. Ionic conductivity and Young's modulus are used to describe the behaviour of the material. However, due to SBE design, as illustrated in Figure 1.5, diffusion counteracts the stiffness of the material. Consequently, higher ion conductivity leads to lower stiffness and vice versa. This is happening because ions are transferred through the liquid phase which exists in the SBE structure. In order for the diffusion of lithium ions to be faster more liquid phase is essential, leading to less space for the solid polymer. This will eventually decrease the stiffness of the SBE. One challenge arises, is the modelling and prediction of these properties due to this counteracting behaviour.

Another challenge for structural battery design is that the SBE interface with the carbon fibres needs to be suitable to support the structure during the operation. A promising process to resolve these challenges is to start with a homogeneous liquid that upon polymerization transform to a heterogeneous material. Initially the components, which are miscible to each other, are mixed and upon solidification/polymerization phase separation takes place. Thermal or UV curing can be used as initiative factor for the polymerization and consequently phase separation. A schematic approach of thermal curing is depicted in Figure 1.5.

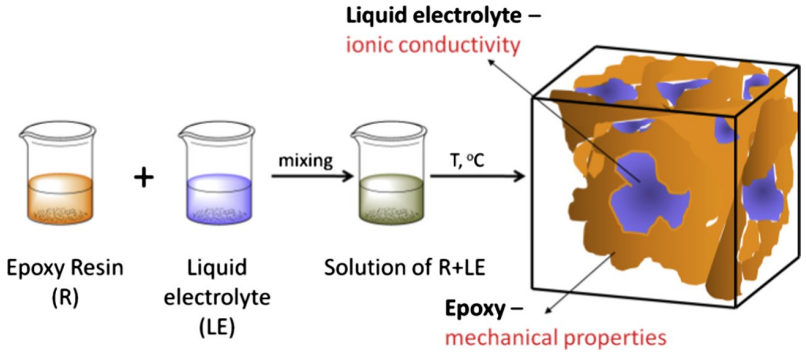

Figure 1.5: Schematic illustration of multifunctional matrices approach presented by Shirshova et al.[17].

The final product is a porous matrix with voids on a sub-micron scale filled with liquid electrolyte. The solid phase determines the mechanical load transfer whereas the liquid controls the ion diffusivity. Scanning Electron Microscopy (SEM) image of a carbon fibre surrounded by the solid phase of SBE is shown in Figure 1.6.

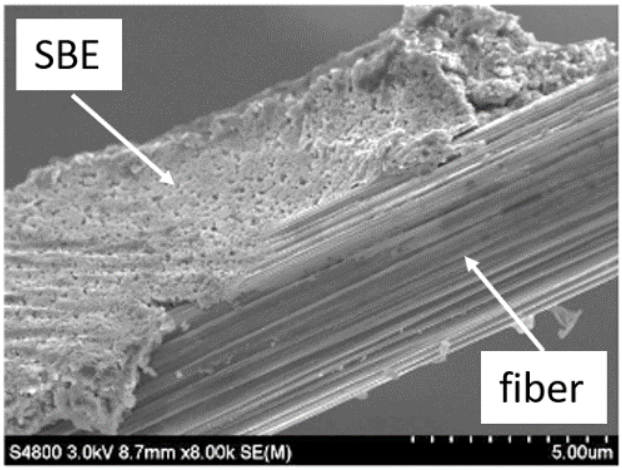

Figure 1.6: SEM images of composite electrode presented by [18].

1.3 Problem Statement and Approach

The current thesis focuses on modelling the deformations in a homogenized porous structural battery electrode of the laminated design, due to mechanical and electrical loads. During the operation of the battery mechanical strains occur because carbon fibres host lithium ions. This process causes an expansion of the fibres, which will further affect stiffness and conductivity, both for the carbon fibre and the surrounding SBE. Low current rates and one lithiation cycle in the carbon fibres are implemented in the current analysis. This simplification has been implemented in order to allow for thermal effects to be neglected. In the present thesis, a micro material model of the structural battery cell and the negative electrode has been formulated and implemented in a square fibre packing array.

2

Theory and Methods

Structural batteries are electrochemical cells, that consist of two electrodes (negative and positive), a separator and the SBE. In the current analysis half cell model are used which alter the conditions because lithium metal is used as electrode. Lithium metal can be considered as an infinite source of lithium ions. A schematic approach of the half cell as implemented in the analysis is depicted in Figure 2.1(left). The domain consists of a carbon fibre, SBE, separator and the lithium metal. During lithiation, lithium ions transport from the lithium metal through the separator, the SBE and finally intercalate in the carbon fibre via diffusion. The electrons are collected and provide the necessary electric energy. Current, electron and ions flows are depicted in the Figure 2.1(right).

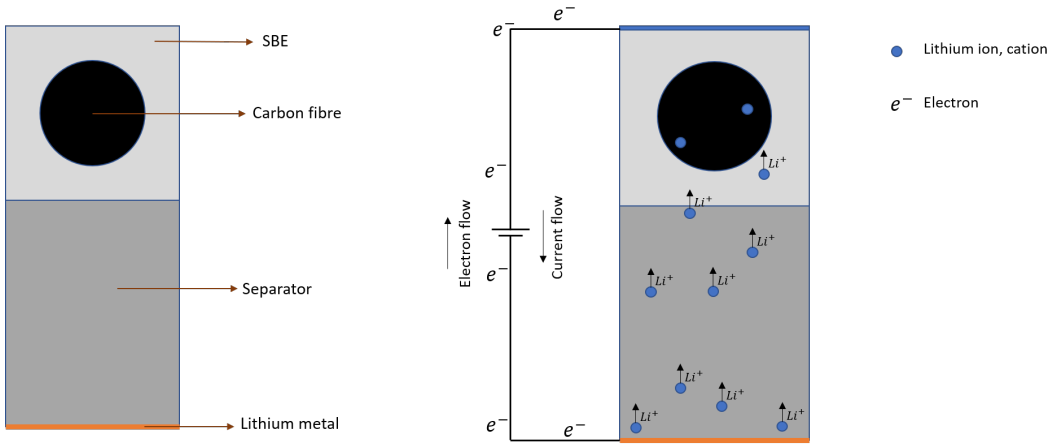

Figure 2.1: (Left) Schematic approach of the half cell model including the necessary domains. (Right) Current, electron and ion flows corresponds to lithiation.

The analysis in the current thesis has been performed on a square fibre packing array, as illustrated in Figure 2.2 and it is one out of two commonly used packing (square and hexagonal packing). However, in order for this packing to be used some assumptions have been made. Firstly, there is a perfect bonding between the fibre and the matrix. Secondly, the fibres are continuous and parallel to each other. Also, the fibres are evenly distributed and each fibre is at an equidistant from another. For this idealised configuration, symmetry and periodicity can be utilised. For that reason, only one array is considered to analyse the lamina with a micro mechanical model. Furthermore, this array represents the arrangement of the fibres in the lamina and for that it is called "Unit cell". This unit cell is what has been used in the current model.

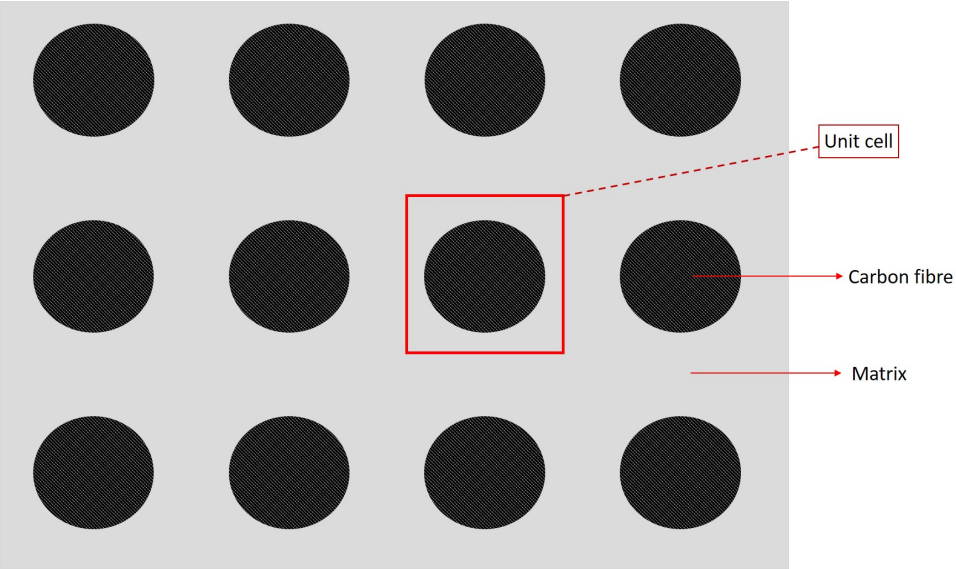

Figure 2.2: Schematic square packing array of a composite material which consists of carbon fibres and a surrounded matrix.

2.1 Redox reactions

Lithium metal and carbon fibres are used. The lithium metal has a lower potential than the carbon fibre and therefore, is the negative electrode, leaving the carbon fibre as positive. During the operation of the battery, reduction and oxidation reactions take place. Reduction involves the gain of an electron and thus a decrease in the oxidation state. Oxidation involves the loss of an electron and thus an increase in the oxidation state. During lithiation phase, the reduction reaction happens at the positive electrode and oxidation at the negative and vice versa during delithiation phase. The following schemes refer to the reduction, oxidation, and overall cell reactions respectively. The parameter χ depends on the carbon fibre and its chemical composition.

$$C_6 + \chi Li^+ + \chi e^- \longrightarrow C_6Li_\chi$$

$$Li_\chi \longrightarrow \chi Li^+ + \chi e^-$$

$$Li_\chi + C_6 \longrightarrow C_6Li_\chi$$

2.2 The COMSOL model

The analysis was performed with the usage of COMSOL Multiphysics 5.5 software. The coupled problems of the electrochemical and mechanical analysis, as Figure 2.3 shows, have been implemented. For the swelling calculations of the fibres, different studies were used, which take place on different domains. The analysis of those studies are analysed in the following subsections. The properties of the materials are in Table A.1 (see Appendix 1).

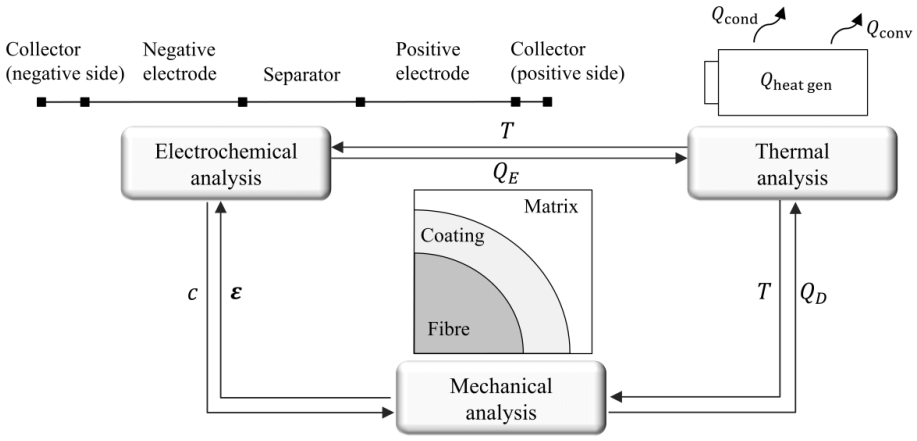

Figure 2.3: Schematic illustration of the coupled problems occur in structural batteries composite [19].

2.2.1 Electrochemical analysis

The evaluation of the electrical performance in the half cell structural battery has been performed via COMSOL built-in modules for electrochemical analysis. The lithium ion battery module in combination with the transport of diluted species module have been used for this reason. Each study has different outcome and dependant variables. The results of the lithium ion module are the current and potential distribution across the cell. The corresponding dependant variables are the electrolyte and electric potential as well as the electrolyte salt concentration. For the transport of diluted species study, the only dependant variable is the lithium concentration and the solution of this analysis is the lithium ion distribution in the carbon fibre. The analysis is based on Newman et al. [20, 21]. The SBE is a porous heterogeneous structure, however homogenized properties have been used for the components of the cell [22]. Mass and charge transport equations are implemented in different domains (electrolyte or solid constituents) to describe the charging phase of the fibre.

2.2.1.1 Carbon fibre

Carbon fibre is the active electrode, which intercalates the lithium ions. The charge balance in this domain is governed by Ohm's law as

$$\nabla \cdot i_s = Q_s \text{ where } i_s = -\sigma_s \nabla \phi_s. \tag{2.1}$$

Subscript s denotes the solid phase (carbon fibre). From this equation, σ_s is the effective electrical conductivity and ϕ_s the electrical potential of the carbon fibre. Also, Q_s is related with the electrical loads, which are interpreted with Butler-Volmer kinematics on the interface between the carbon fibre and the SBE. The corresponding equations are presented and discussed in the following subsections. In this domain the mass transport equation takes place given by

$$\frac{\partial c_i}{\partial t} + \nabla J_i = R_i. \tag{2.2}$$

In the Equation 2.2, c_i is the concentration field of any species, which in this analysis corresponds to the lithium ion. The analysis is not stationary meaning that the concentration field changes with time, and is affected by the electrical field. The transport of the lithium is a coupled problem with the current and potential distribution. Any change at one of the studies affect the other. For the flux J_i, Fick's law has been used, where

$$J_i = -D_i \nabla c_i. \tag{2.3}$$

D_i corresponds to the diffusion coefficient of the carbon fibre as Table A.1 shows.

2.2.1.2 Structural Battery Electrolyte and Separator

The material balance equation is applied on this domain to express the conservation of mass

$$\frac{\partial c_l}{\partial t} + \nabla \cdot J_l = R_l \tag{2.4}$$

$$J_l = -D \nabla c_l + \frac{i_l t_+}{F}. \tag{2.5}$$

Also, the charge balance equations which takes place in the electrolyte phase is given by the following expression

$$\boldsymbol{i_l} = -\sigma_l \nabla \phi_l + \frac{2\sigma_l RT}{F}(1 - t_+) \nabla \ln c_l \tag{2.6}$$

where σ_l is the effective ion conductivity, ϕ_l the potential and c_l the lithium salt concentration. The subscript l corresponds to the electrolyte phase. The parameter t_+ indicates the fraction of the total electrical current in the electrolyte carried from the ionic species (Li^+). This term is called transport number. In Equation 2.6, $\boldsymbol{i_l}$ corresponds to the average current density. Bulter-Volmer kinematics are used to define this term in the following subsection. Finally, T, R and F represent the temperature, universal gas constant (8.314 [$JK^{-1}\text{mol}^{-1}$]) and Faraday's constant (96485.3329[C/mol]), respectively.

Charge balance and material balance relations (Equations 2.4-2.6) are valid in the separator domain, like in the SBE. However, in this region tortuosity must be taken into account. Tortuosity is a parameter which significantly influences the transfer of particles in porous media, such as the separator. It occurs, due to the irregular paths lithium ions are forced to follow, leading to reduction in the conductivity. For this reason the Equation 2.6 have to be revised regarding the ion conductivity and diffusion coefficients. For this purpose Bruggeman correction factor has been introduced and the effective properties are

$$\sigma_{l,eff} = \sigma_l \, \epsilon_l^{\beta} \quad \text{and} \quad D_{l,eff} = D_l \, \epsilon_l^{\beta}. \tag{2.7}$$

From Equation 2.7, β is the Bruggeman coefficient and ϵ_l the electrolyte volume fraction. These values can be seen in the Table A.1.

2.2.1.3 Charge transfer (electrode and electrolyte interface)

For the charge transfer reaction, Butler-Volmer kinetics are implemented as follows

$$I = i_0 \left[\exp\left(\frac{a_a F \eta_s}{RT}\right) - \exp\left(\frac{-a_c F \eta_s}{RT}\right) \right] \tag{2.8}$$

where I is the superficial current density [21]. This parameter also, represents the rate of oxidation (corrosion) and reduction (decomposition). η_s is the local surface over-potential value, which is defined as $\eta_s = E_{ect} - E_{eq} = \phi_s - \phi_l - E_{eq}$. The electric potential for the electrode and electrolyte phase refers as ϕ_s, ϕ_l respectively. The E_{eq} is the equilibrium potential of the electrode. Also, α_a and α_c refer to the anodic and cathodic transfer coefficients. Both α_a and α_c are related with the reduction and oxidation reactions respectively. These coefficients indicate the fraction of the electrode potential involved in each reaction. Finally, i_0 corresponds to the exchange current density, which characterises the electrochemical processes, and sets the over-potential to zero, $\eta_s = 0$.
At equilibrium, anodic and cathodic currents are equal in magnitude and correspond to the exchange current, i_0. However, during the operation of the battery there is a deviation of the electrode potential from the equilibrium potential. This deviation is called over-potential and denotes the term n_s.

2.2.2 Solid mechanics

The mechanical response of the half cell has been evaluated, in order to predict the swelling of the fibre. For this analysis the solid mechanics study from COMSOL software has been used, and the dependant variables are those related to the displacement field. During lithiation, lithium ions intercalate into the microstructure of the fibre, making the lattice to expand. This expansion is responsible for the compression of the surrounding SBE, which affects the ion conductivity an matrix dominated elastic properties of the structural battery. The solid mechanics study has been applied in the fibre domain where a linear elastic response has been implemented. The governing balance equation is

$$-\nabla \cdot \boldsymbol{S} = \boldsymbol{b}. \tag{2.9}$$

The term $\boldsymbol{S}$ corresponds to the stresses applied on this domain. The symbol $\boldsymbol{\sigma}$ is commonly used for the stress tensor, however for the current analysis $\boldsymbol{S}$ replaced this, to prevent any confusion with the ion conductivity term from the previous studies. The term $\boldsymbol{b}$ represents the body forces in the selected domain. The outcome of the solid mechanics study is the displacement field, and afterwards the strains are evaluated. The mechanical response is coupled with the electrochemical model, which gives rise to an additional strain term. This term is called electrochemical strain and appears due to the lithium intercalation.

For an composite material the total mechanical strain is calculated as follows

$$\epsilon^M = \epsilon - \epsilon^T - \epsilon^H, \tag{2.10}$$

where ϵ is the elastic strains , ϵ^T the thermal strains which are neglected in the current analysis and ϵ^H the hygroscopic strain. However, the battery cell is been protected from the outer environment via a pouch bag to prevent any moisture insertion. Hence, ϵ^H is zero. For this reason, the total mechanical strain has been redefined as

$$\epsilon^M = \epsilon - \epsilon^T - \epsilon^E, \tag{2.11}$$

where the ϵ^E is the electrochemical strain. This strain has been computed as

$$\epsilon^E = \mu \Delta \overline{C}. \tag{2.12}$$

In Equation 2.12, μ, is the expansion coefficient due to lithium intercalation and $\overline{C}$ represents the normalised lithium concentration in the fibre (active electrode) as

$$\overline{C} = \frac{C}{C_{sat}}. \tag{2.13}$$

The term C corresponds to the lithium concentration in every timestep and C_{sat} is the saturated lithium concentration (maximum value of lithium ions that carbon fibre can host).
The stress state arises in the domain is expressed as

$$\boldsymbol{S} = \overline{\boldsymbol{Q}} : \boldsymbol{\epsilon^M}. \tag{2.14}$$

The boundary conditions used in the current analysis are depicted on the Figure 2.4.

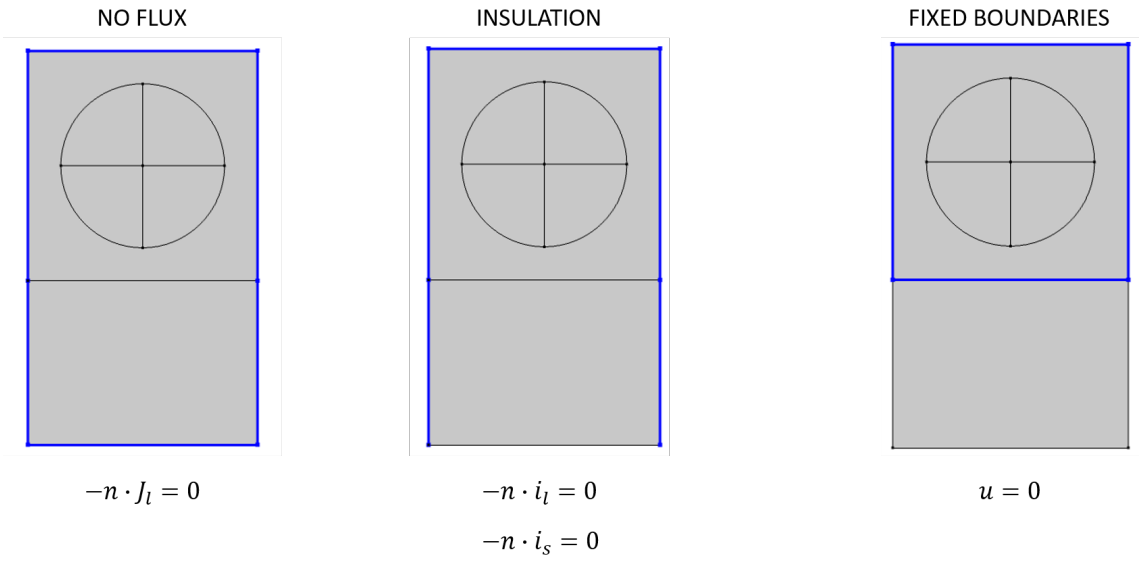

Figure 2.4: Boundary conditions for the applied studies.

The blue lines represent the boundaries where the constraints are applied. The subscript l and s corresponds to the liquid and solid phase, respectively. To summarise the equations, a schematic of the geometry with the applied equations are depicted in Figure 2.5.

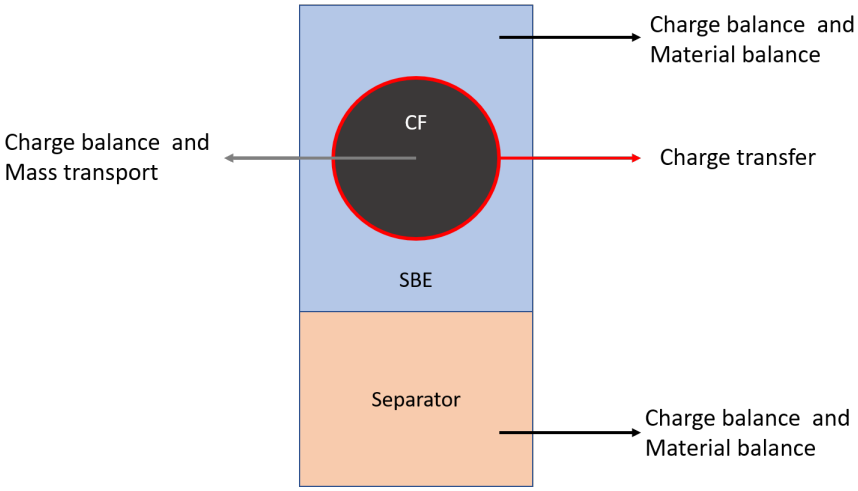

Figure 2.5: Applied governing equations on the different domains.

2.3 Porosity dependant properties

The aim is to predict the properties of the SBE due to the deformations occurred during the swelling of the carbon fibre. These properties are functions of the porosity in the SBE. However, the porosity changes over time depending on the state of charge (SOC) of the fibre. Virtual tests have been performed by Tu [22], for different types of microstructures. These tests show the relation between the Young's modulus and ion conductivity as a function of porosity, as shown in Figure 2.6.

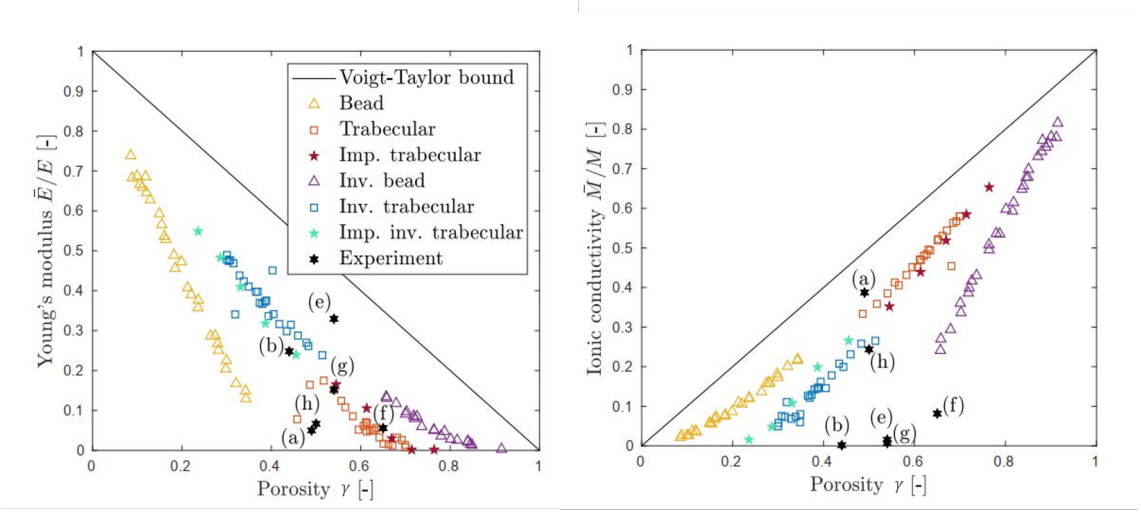

Figure 2.6: Illustration of the dependency of the Young's modulus (left) and ion conductivity (right) versus the porosity of the SBE [22].

The data used in the current thesis are those corresponds to the so called imperfect trabecular microstructure (symbolised with red star marker). These microstructures were generated from Tu [22] with usage of the Cahn-Hilliard equation, which is a fourth order differential equation and describes the phase separation [23, 24]. In the present analysis the porosity is linked to the strains which are functions of the time, $\gamma[\epsilon(t)]$. A linear relation between strains developed in the SBE and the porosity is introduced

$$\gamma = \kappa \boldsymbol{\epsilon} = \kappa \nabla \boldsymbol{u}, \tag{2.15}$$

where $\boldsymbol{u}$ is the displacement field which is calculated from the solid mechanics study in COMSOL software. The initial porosity of the SBE is $\gamma_{in} = 0.38$ when the strains are zero, and set to zero as soon as the threshold strain reach $\epsilon_{thr} = 0.30$. From the approximated linear relation of these quantities Equation 2.16 is implemented

$$\gamma = -a \cdot \epsilon_{vol} + b = -\frac{\gamma_{in}}{\epsilon_{thr}} \cdot \epsilon_{vol} + \gamma_{in}. \tag{2.16}$$

The volumetric strain has been computed as

$$\frac{\Delta V}{V_0} = \frac{V - V_0}{V_0} = \frac{(a + \Delta a)(b + \Delta b) - ab}{ab} = \epsilon_{xx} + \epsilon_{yy} \tag{2.17}$$

The volumetric strains are evaluated for a material element which has normally deformed without shear, see Figure 2.7. To include shearing strains an additional term, $\epsilon_{xx}\epsilon_{yy}$ is rising.

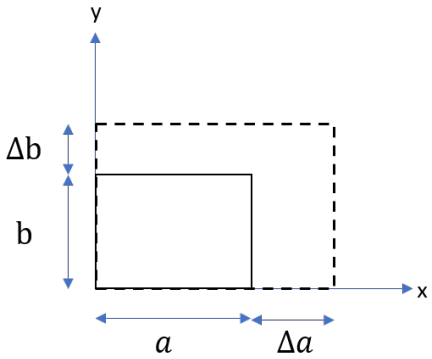

Figure 2.7: Normal deformation of a material element, without shearing.

Figure 2.8 displays a plot which shows the linear relation between the porosity and the volumetric strain.

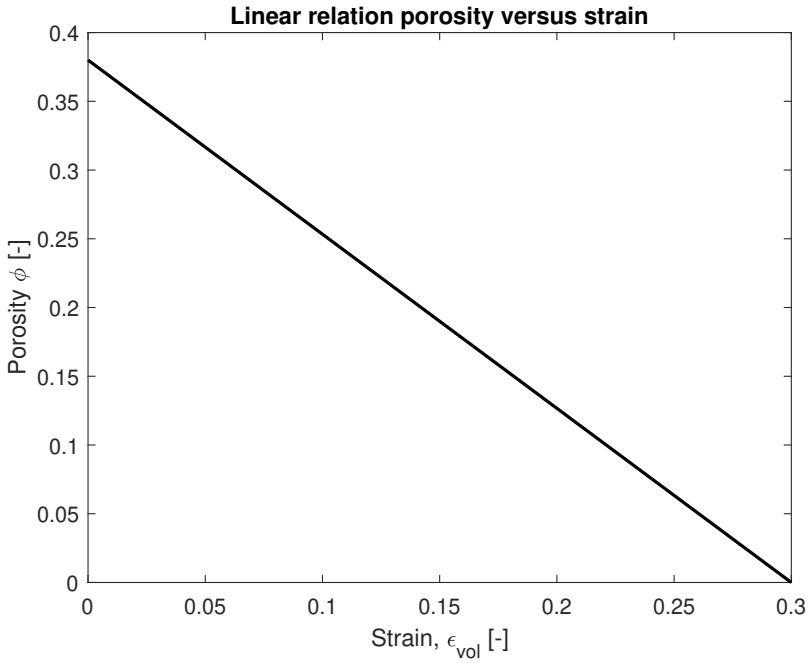

Figure 2.8: Linear relation between porosity and volumetric strain.

From Figure 2.8 is clear that as soon as the strain increases the porosity decreases. At each timestep the strains are calculated and the porosity is evaluated, which is used to update the Young's modulus and the ion conductivity from Tu's plots (Figure 2.6) . However, in order to extract the approximated properties of the SBE an normalised porosity is introduced. The range of values of Equation 2.16 is $[0, \gamma_{in} = 0.38]$. In order to adjust these values, the initial porosity to normalise them has been used. The equation of the porosity in that case has been evaluated as

$$\gamma_{norm} = \frac{\gamma}{\gamma_{in}} = -\frac{1}{\epsilon_{thr}} \cdot \epsilon_{vol} + 1. \tag{2.18}$$

2.4 State of charge dependant properties

The profiles of lithium ion distribution in the fibre have been evaluated. An important parameter for the diffusion equation is the diffusion coefficient which is a function of the state of charge of the fibre. The data for that coefficient as well as the exchange current density have been extracted from Kjell et al. [25].

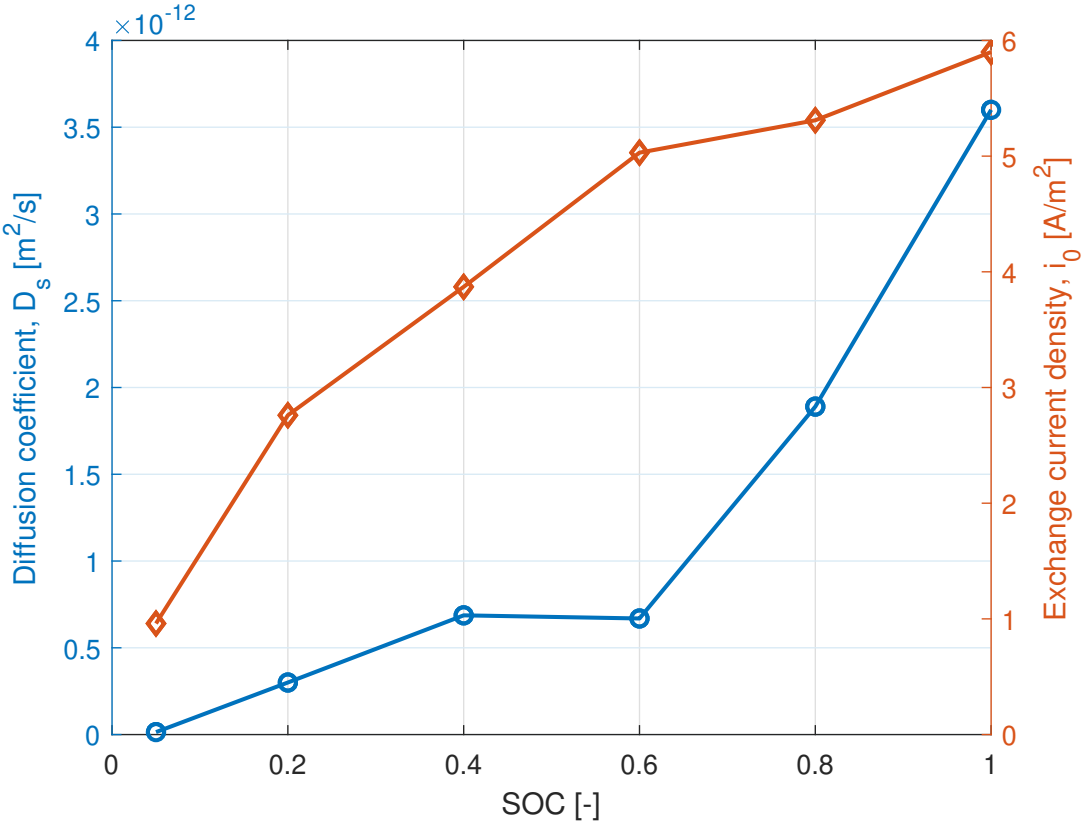

Figure 2.9: Diffusion coefficient and exchange current density as function of the state of charge of the fibre.

The red line represents the exchange current density in Butler-Volmer kinetics Equation 2.8, whereas the blue corresponds to the diffusion coefficient. As the lithiation state increases the coefficient increases as well, leading to enhanced diffusion. This is happening because lithium ions interact with the microstructure as intercalation takes place, and creates space between the carbon layers of the fibre.

3

Results

3.1 Electrochemical analysis

One cycle of lithiation has been performed on the half cell model. The fibre is considered to be fully lithiated for voltages below 0.08 V vs Li/Li^+ and delithiated at 1.5 V vs Li/Li^+. Figure 3.1 shows the external electric potential, of the half cell during the lithiation of the fibre. The current rate used for the simulations is $1C$, meaning that $1h$ is needed for the fibre to be fully lithiated.

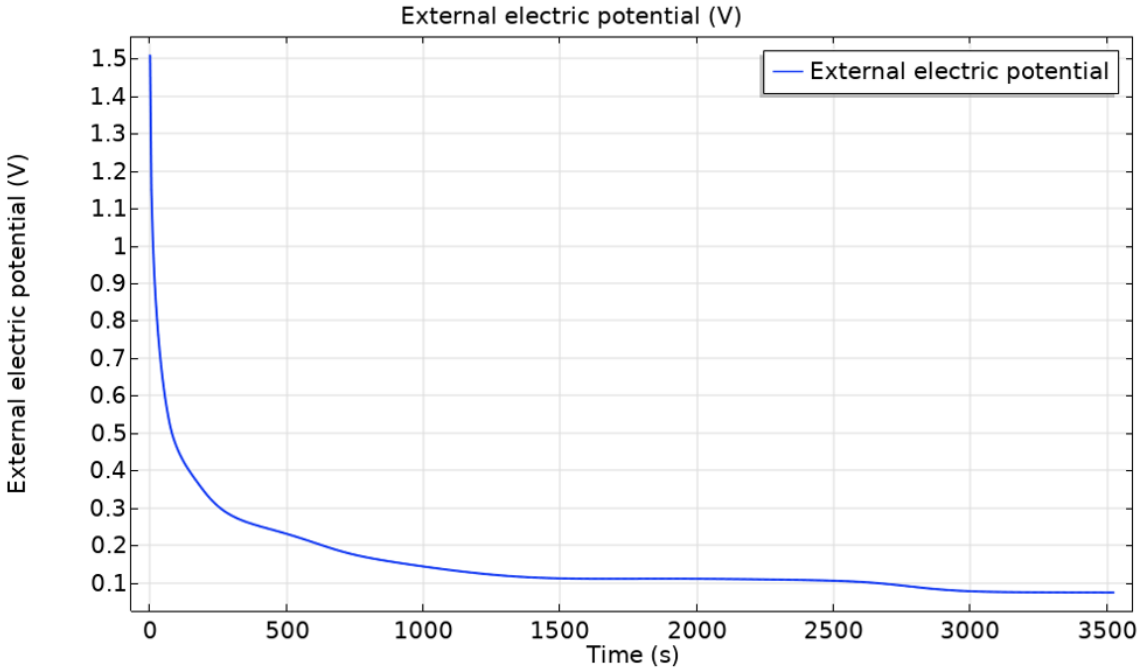

Figure 3.1: External electric potential of the carbon fibre.

A contour plot of the concentration field is shown in Figure 3.2. Lithiation causes the fibre to expand which leads to the compression of the surrounding SBE. The concentration of Li^+ is almost uniform across the fibre domain and the state of charge is 99%. The volume fraction of the fibre in the Figure 3.2 is $V_f = 40\%$.

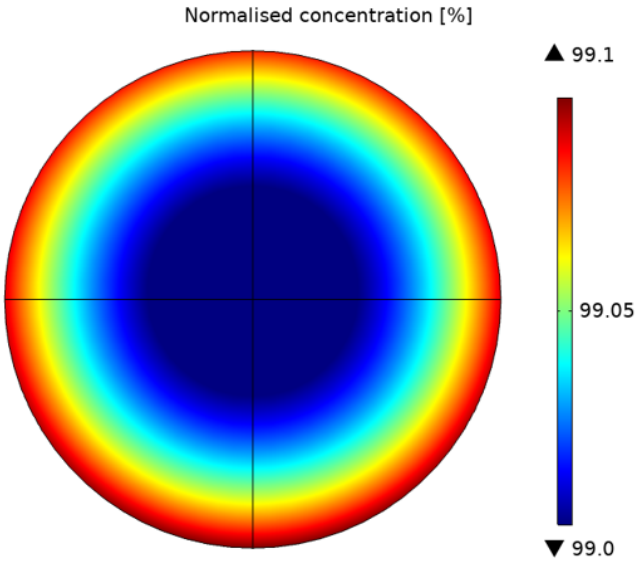

Figure 3.2: Concentration field of lithium ions in the lithiated carbon fibre domain, for a volume fraction of $V_f = 40\%$.

3.2 Solid mechanics

From the solid mechanics study the electrochemical strains on the CF domain are evaluated. A schematic of these strains on a fibre with volume fraction $V_f = 40\%$ is shown below.

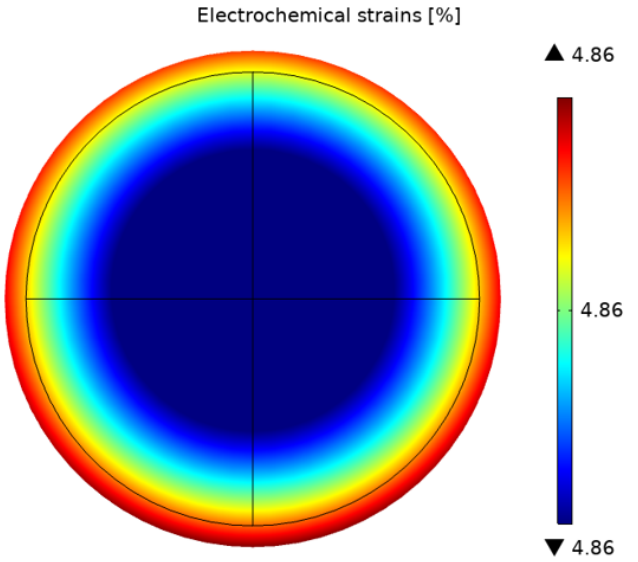

Figure 3.3: Electrochemical strains on a lithiated fibre with volume fraction $V_f = 40\%$.

The black circle represents the initial shape of the fibre. The coloured domain illustrates the deformed region due to the intercalation of the lithium ions. The electrochemical swelling has been evaluated to $\epsilon_{max} = 4.86\%$ at the radial direction.

3.3 Parametric study

A parametric study for various volume fractions of the fibres has been performed. The fibre volume fraction ranges from $V_f = 30\%$ to $V_f = 60\%$. The radius of the fibre was kept constant, and the length of the half cell changed for each V_f.

$$V_f = \frac{Area_{fibre}}{Area_{SBE}} \Rightarrow Lsq = \sqrt{\frac{\pi r_f^2}{V_f}} \tag{3.1}$$

where Lsq represents the length of the half cell, and r_f the radius of the fibre, as shown in Figure 3.4.

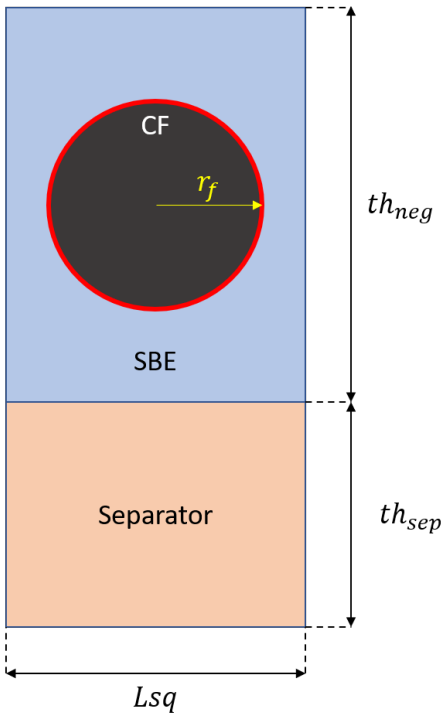

Figure 3.4: Dimensions used to describe the half cell model.

The concentration of Li^+ in the fibre has been evaluated for various volume fractions, as shown in Figure 3.5. The line graphs, represent the concentration across the radius of the fibre. The x-axis in Figure 3.5 represents the normalised length of the fibre, and the y-axis the normalised concentration. All curves corresponds to profiles, which are extracted on the same time-step, $t = 3505\ s$ for a lithiated fibre. As the volume fraction increases the concentration profile is almost identical.

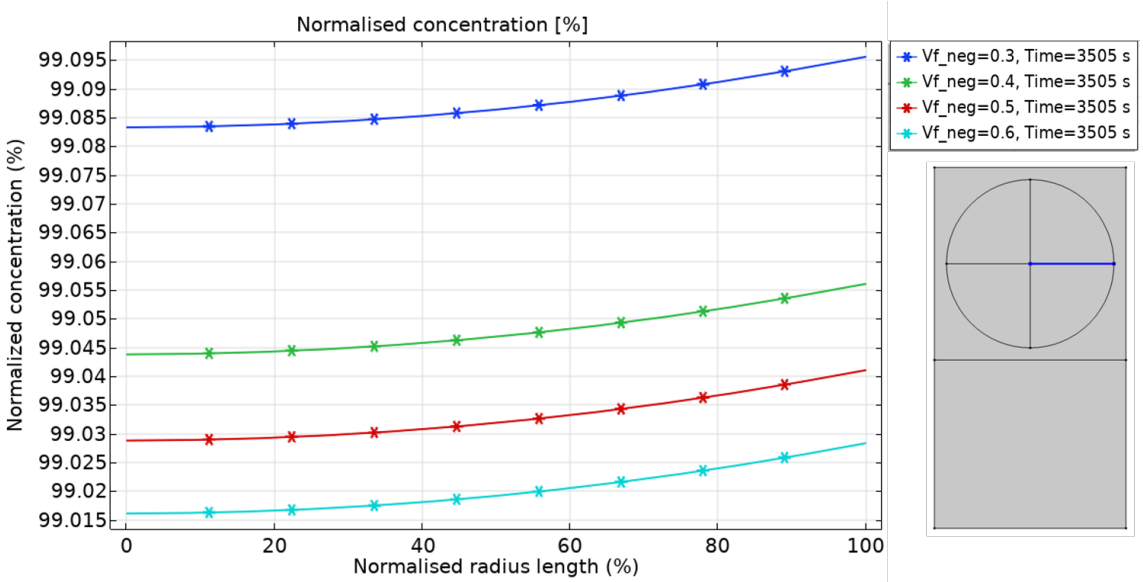

Figure 3.5: Concentration profile across the radius of the fibre form different volume fractions.

The curves indicate small differences between the centre and circumferential positions of the fibre. This uniform distribution of lithium ions in the domain implies that there are no stress gradients.

The swelling of the lithiated fibre has to be evaluated, because it will affect the electrochemical properties of the surrounding SBE. The expansion of the fibre for each volume fraction is the same, since the differences in lithium concentration is negligible as shown in Figure 3.5. However the surrounding SBE is affected differently for each fibre volume fraction. The resulting volumetric strains in the SBE for the different volume fractions are shown in Figure 3.6a-3.6d.

The initial shape of the fibre corresponds to the black circle and the final deformation can be seen from the white circle. As the volume fraction increases the computed volumetric strains are increasing dramatically. Different areas are shown on the plots, which represent the magnitude of the strains. The blue areas corresponds to the most affected zones. For $V_f = 30\%$ the maximum volumetric strains are calculated to $\epsilon_{max} = -5.72\%$. The minus sign corresponds to the compressive loads and the strains has been measured in percentages. The maximum calculated strains differs for each volume fraction. For $V_f = 40\%$ the compression is around -9%, for $V_f = 50\%$ is -15% and finally for $V_f = 60$ the strains take values up to -29.8%. The red areas correspond to the least affected areas. The developed strains, and the distribution of them however, are affected from the boundary conditions used for the model. The strains developed on the SBE are cause a change in porosity, as shown in Figure 3.7a-3.7d.

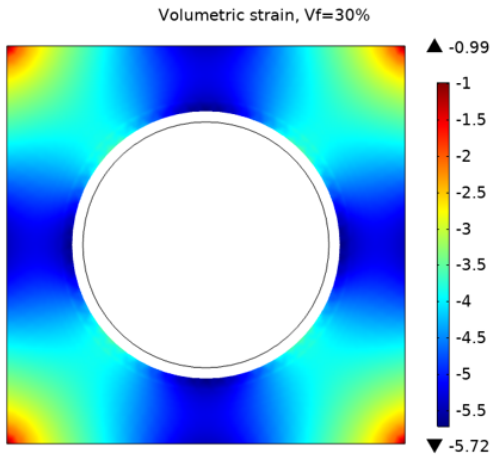

(a) $V_f = 30\%$

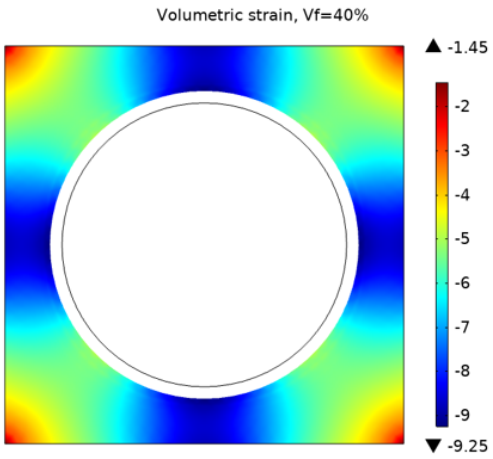

(b) $V_f = 40\%$

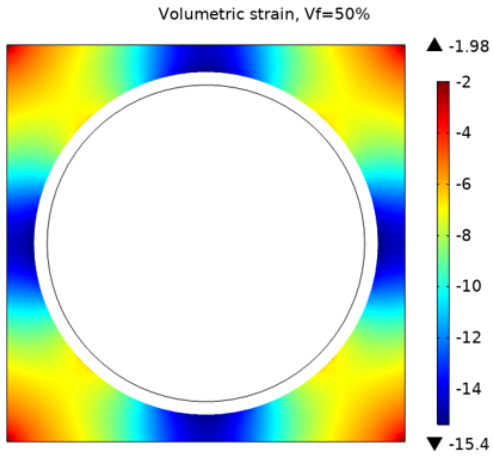

(c) $V_f = 50\%$

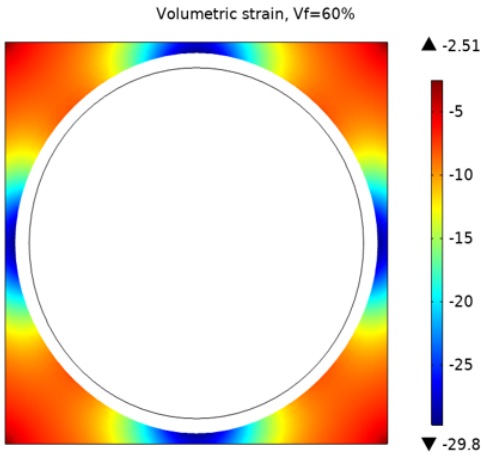

(d) $V_f = 60\%$

Figure 3.6: Volumetric strains in SBE domain for different fibre volume fraction

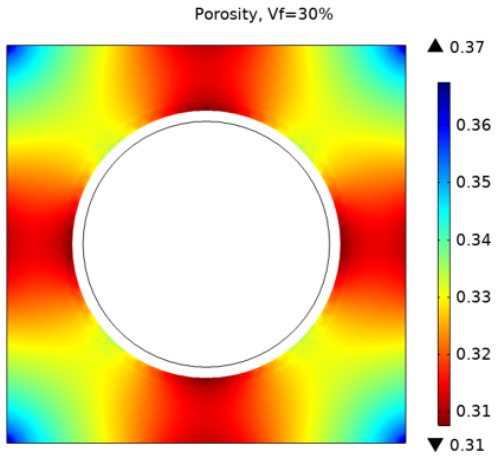

(a) $V_f = 30\%$

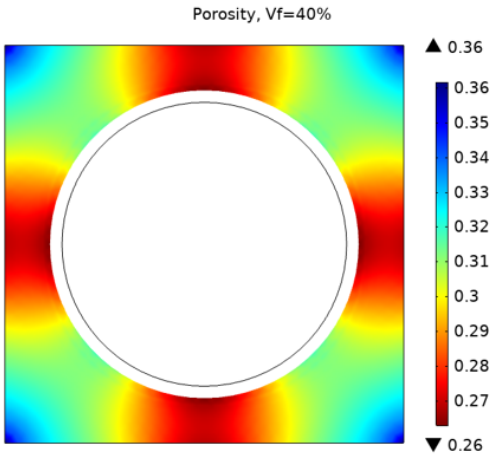

(b) $V_f = 40\%$

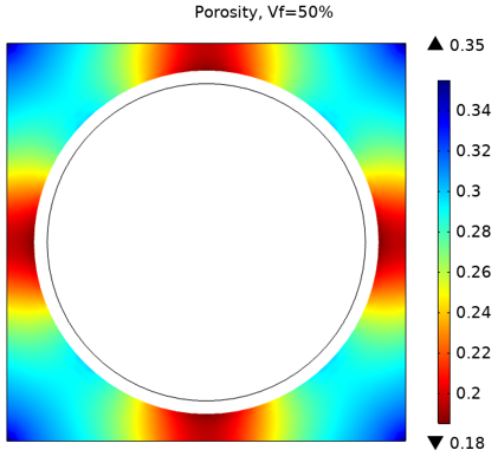

(c) $V_f = 50\%$

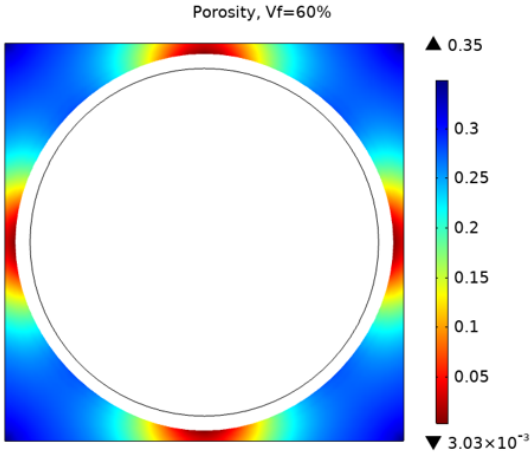

(d) $V_f = 60\%$

Figure 3.7: Porosity in the SBE for different fibre volume fraction

Highly affected areas are illustrated in red, whereas blue has been used for the least. Equation 2.16 has been used for the evaluation of the porosity. The porosity assumed to have a linear relation with the volumetric strain. For that reason it follows the same trend. For $V_f = 30\%$ the porosity drops down to 31% over a larger area (red areas). This porosity decay has a more even distribution across the SBE domain in comparison with the other volume fraction. In particular, for $V_f = 40\%$ there are areas with 26% porosity, for $V_f = 50\%$ the affected areas has 18% and finally for $V_f = 60\%$ the porosity is almost 0.8%. However the unaffected zones when the volume fraction is higher seems to be larger. As mentioned before, these values are related with the boundary conditions used for the modelling.

The porous SBE is the medium which allows lithium ions to transport between the electrodes. As the porosity decreases the available cavities which contains the considering electrolyte close. Consequently, the ion conductivity will be reduced. Considering Tu's data [22], an ion conductivity knock-factor is presented in Figures 3.8a-3.8d.

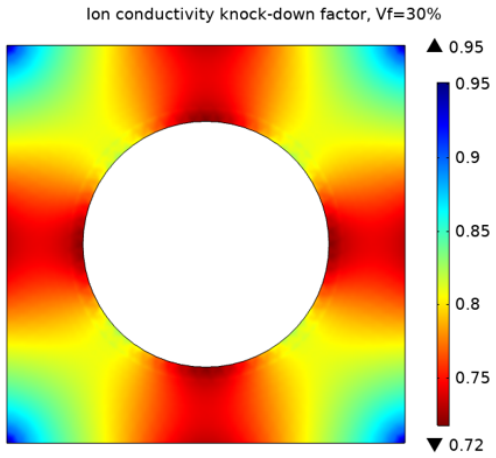

(a) $V_f = 30\%$

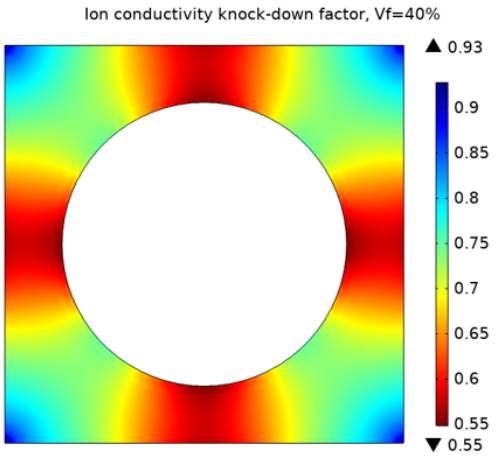

(b) $V_f = 40\%$

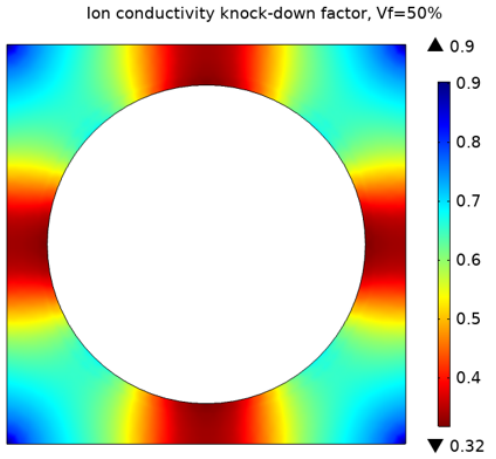

(c) $V_f = 50\%$

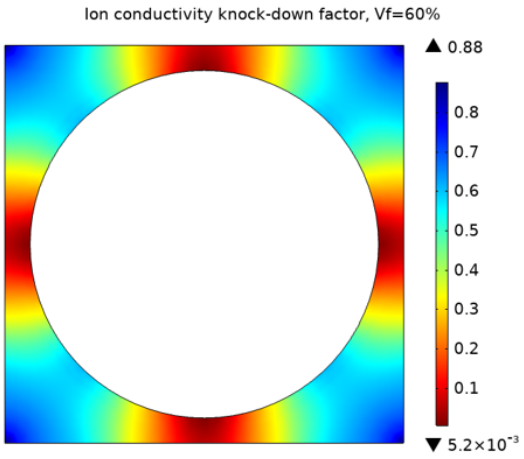

(d) $V_f = 60\%$

Figure 3.8: Ion conductivity knock-down factor in SBE for different fibre volume fractions

A vertical path from top to bottom of the SBE in the unit cell has been created as shown in Figure 3.9 and the average ion conductivity has been evaluated.

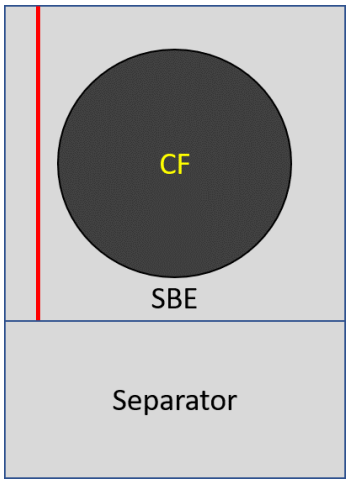

Figure 3.9: Line of interest for ion conductivity data extraction.

For the various volume fractions the effect on the ion conductivity is depicted in Figure 3.10.

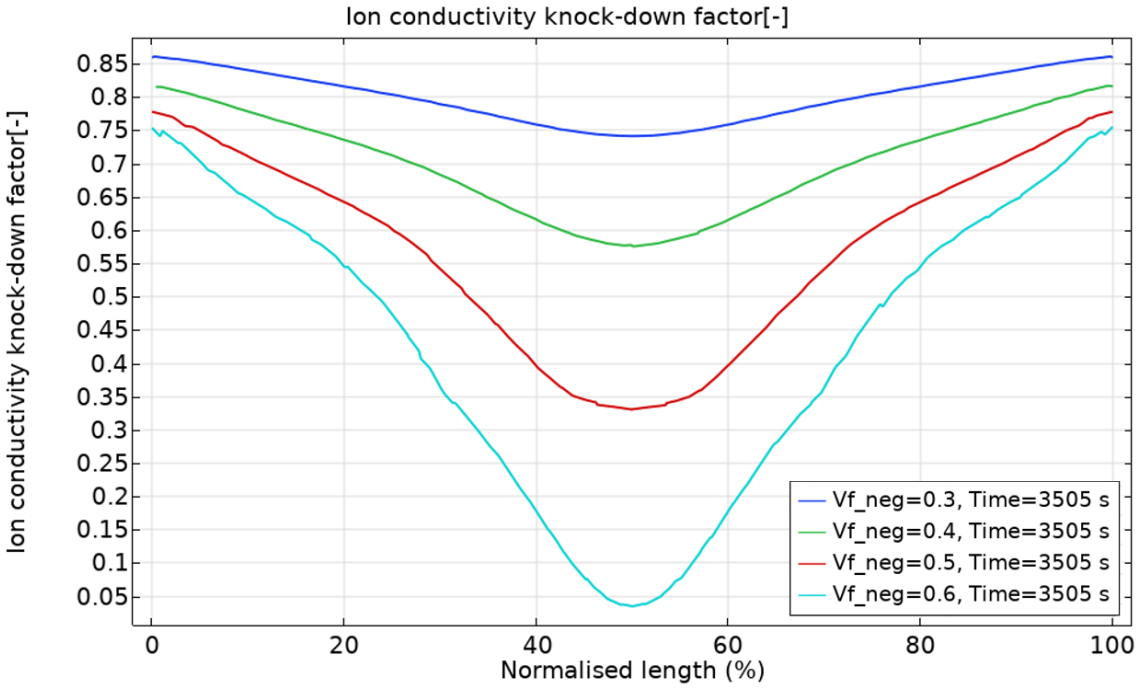

Figure 3.10: Avarage ion conductivity across the SBE for the different volume fractions of the carbon fibre.

The x-axis corresponds to the normalised path length as Figure 3.9 shows. From the plot it is clear that the ion conductivity is affected the most in the middle of the line where the fibre and the boundary has the least available space for expansion. Significant sharp behaviour is shown as the volume fraction increases. A schematic of the positive ion flux through the SBE is shown with black arrows in Figure 3.11.

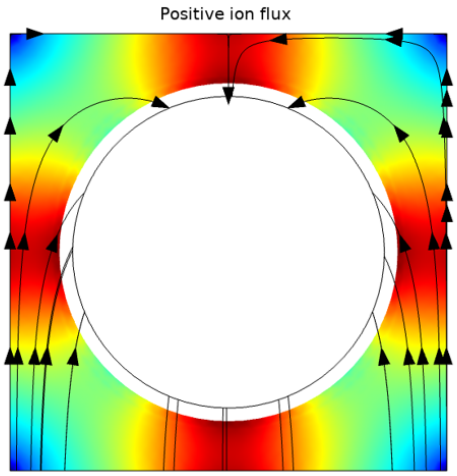

Figure 3.11: Schematic of the positive ion flux in the SBE.

The ion conductivity is an important property of the SBE because it shows the ability to transport lithium ions. In order for these cations to be intercalated in the carbon fibre microstructure, transport through the highly affected zones is necessary. Taking the square packing of the fibre into account, as Figure 2.2 shows, the ions have to be able to transport in the other fibre across the electrode. That means, high values of fibre volume fractions needs to be avoided as the lithium transportation becomes more difficult.

4
Conclusion

In order to study the effect on the electrochemical properties in a porous structural battery electrolyte (SBE), an electrochemical cell consisting of carbon fibres embedded in SBE versus lithium metal was modelled. The model was established in COMSOL to simulate the electrochemical and mechanical behaviour during lithiation. The FE model was developed based on the governing equations defined in section 2.2.
The SBE is composed by a solid polymer network with liquid electrolyte filled pores. The role of the SBE in the structural battery is to transfer load and enable ions to be transported between the electrodes. Both mechanical and transport properties of the SBE are affected by the change in porosity, due to the associated volume change in the fibre during lithiation.
Results show a 5% radial expansion on the fibre which leads to compression of the surrounded SBE. The volumetric strains occur in the SBE are highly affected of the porosity and the volume fraction of the carbon fibre. Parametric study of the fibre's volume fraction has been conducted. The knock-down factor for the ion conductivity of the SBE is computed which takes values to almost 0.8% when the volume fraction reaches 60%. This implies that dense electrodes needs to be avoided. However, the analysis is conducted for linear elastic materials and fixed boundary condition. Different material models and boundary conditions would have been interesting to be investigated in the future. The threshold value of porosity is an important parameter which needs further experimental research. This will also help the validation and calibration of the model.
Many impediments were encountered and compromises were made during the project. Concluding, that denser arrays will decrease the electrochemical performance of the structural batteries, due to the high volumetric strains occurred on the SBE. Pores will close during lithiation and the lithium ions will be unable to be transported.

Bibliography

[1] Johanna Xu et al. "Characterization of the adhesive properties between structural battery electrolytes and carbon fibers". In: *Composites Science and Technology* 188.December 2019 (Mar. 2020). ISSN: 02663538. DOI: 10.1016/j.compscitech.2019.107962.

[2] Maria H. Kjell et al. "PAN-Based Carbon Fiber Negative Electrodes for Structural Lithium-Ion Batteries". In: *Journal of The Electrochemical Society* 158.12 (2011), A1455. ISSN: 00134651. DOI: 10.1149/2.053112jes.

[3] Eric Jacques et al. "Impact of electrochemical cycling on the tensile properties of carbon fibres for structural lithium-ion composite batteries". In: *Composites Science and Technology* 72.7 (Apr. 2012), pp. 792–798. ISSN: 02663538. DOI: 10.1016/j.compscitech.2012.02.006. URL: http://dx.doi.org/10.1016/j.compscitech.2012.02.006.

[4] Eric Jacques et al. "The effect of lithium-intercalation on the mechanical properties of carbon fibres". In: *Carbon* 68 (Mar. 2014), pp. 725–733. ISSN: 00086223. DOI: 10.1016/j.carbon.2013.11.056.

[5] Yalin Yu et al. "Multifunctional structural lithium ion batteries based on carbon fiber reinforced plastic composites". In: *Composites Science and Technology* 147 (July 2017), pp. 62–70. ISSN: 02663538. DOI: 10.1016/j.compscitech.2017.04.031. URL: http://dx.doi.org/10.1016/j.compscitech.2017.04.031.

[6] Eric D. Wetzel. "Reducing weight: Multifunctional composites integrate power, communications, and structure". In: *AMPTIAC Q* 8.4 (2004), pp. 91–95.

[7] James F. Snyder, Robert H. Carter, and Eric D. Wetzel. "Electrochemical and mechanical behavior in mechanically robust solid polymer electrolytes for use in multifunctional structural batteries". In: *Chemistry of Materials* 19.15 (July 2007), pp. 3793–3801. ISSN: 08974756. DOI: 10.1021/cm070213o.

[8] Giulia Fredi et al. "Graphitic microstructure and performance of carbon fibre Li-ion structural battery electrodes". In: *Multifunctional Materials* 1.1 (Aug. 2018), p. 015003. DOI: 10.1088/2399-7532/aab707.

[9] Tony Carlson. *Multifunctional composite materials – design, manufacture and experimental characterisation, Doctoral Thesis*. 2013. ISBN: 9789174397048. URL: http://www.ucs.iastate.edu/mnet/_repository/2010/ses2010/pdf/abstractbook.pdf#page=329.

[10] Eric D. Wetzel et al. "Multifunctional Structural Power and Energy Composites for U.S Army Applications". In: *Multifunctional Structures / Integration of Sensors and Antennas* 2006 (2006), pp. 2–14. URL: http://www.dtic.

mil/cgi-bin/GetTRDoc?AD=ADA479859%20http://www.rto.nato.int/abstracts.asp..

[11] S. Ekstedt, M. Wysocki, and L. E. Asp. "Structural batteries made from fibre reinforced composites". In: *Plastics, Rubber and Composites* 39.3-5 (June 2010), pp. 148–150. ISSN: 14658011. DOI: 10.1179/174328910X12647080902259.

[12] Tony Carlson. "Multifunctional Composite Materials Design, Manufacture and Experimental Characterisation". In: ISBN: 978-91-7439-705-5.

[13] Leif E. Asp and Emile S. Greenhalgh. "Structural power composites". In: *Composites Science and Technology* 101 (Sept. 2014), pp. 41–61. ISSN: 02663538. DOI: 10.1016/j.compscitech.2014.06.020. URL: http://dx.doi.org/10.1016/j.compscitech.2014.06.020.

[14] David Carlstedt. *THESIS FOR THE DEGREE OF LICENTIATE OF ENGINEERING On the multifunctional performance of structural batteries*. Tech. rep.

[15] N. Ihrner et al. "Structural lithium ion battery electrolytes: Via reaction induced phase-separation". In: *Journal of Materials Chemistry A* 5.48 (2017), pp. 25652–25659. ISSN: 20507496. DOI: 10.1039/c7ta04684g.

[16] Lynn M. Schneider et al. "Bicontinuous Electrolytes via Thermally Initiated Polymerization for Structural Lithium Ion Batteries". In: *ACS Applied Energy Materials* 2.6 (June 2019), pp. 4362–4369. ISSN: 25740962. DOI: 10.1021/acsaem.9b00563.

[17] Natasha Shirshova et al. "Structural supercapacitor electrolytes based on bicontinuous ionic liquid-epoxy resin systems". In: *Journal of Materials Chemistry A* 1.48 (Dec. 2013), pp. 15300–15309. ISSN: 20507488. DOI: 10.1039/c3ta13163g.

[18] Lynn M. Schneider et al. *Bicontinuous Electrolytes via Thermally Initiated Polymerization for Structural Lithium Ion Batteries*. 2019. DOI: 10.1021/acsaem.9b00563.s001. URL: https://acs.figshare.com/articles/Bicontinuous_Electrolytes_via_Thermally_Initiated_Polymerization_for_Structural_Lithium_Ion_Batteries/8171174/1.

[19] N O N Peer Reviewed. "Unit Cells for Multiphysics Modelling of Structural". In: (2019).

[20] John Newman and William Tiedemann. "Porous-electrode theory with battery applications". In: *AIChE Journal* 21.1 (1975), pp. 25–41. DOI: 10.1002/aic.690210103. URL: https://aiche.onlinelibrary.wiley.com/doi/abs/10.1002/aic.690210103.

[21] Marc Doyle. "Modeling of Galvanostatic Charge and Discharge of the Lithium Polymer Insertion Cell". In: *Journal of The Electrochemical Society* 140.6 (1993), p. 1526. DOI: 10.1149/1.2221597. URL: https://iopscience.iop.org/article/10.1149/1.2221597.

[22] Vinh Tu. *Modeling and Finite Element Simulation of the Bifunctional Performance of a Microporous Structural Battery Electrolyte*. Tech. rep.

[23] D. Carolan et al. "Co-continuous polymer systems: A numerical investigation". In: *Computational Materials Science* 98 (Feb. 2015), pp. 24–33. ISSN: 09270256. DOI: 10.1016/j.commatsci.2014.10.039. URL: http://dx.doi.org/10.1016/j.commatsci.2014.10.039.

[24] Christopher Grant. “Spinodal decomposition for the cahn-hilliard equation”. In: *Communications in Partial Differential Equations* 18.3-4 (Jan. 1993), pp. 453–490. ISSN: 15324133. DOI: 10.1080/03605309308820937.

[25] Maria H. Kjell et al. “Electrochemical Characterization of Lithium Intercalation Processes of PAN-Based Carbon Fibers in a Microelectrode System”. In: *Journal of The Electrochemical Society* 160.9 (2013), A1473–A1481. ISSN: 0013-4651. DOI: 10.1149/2.054309jes.

A

Appendix 1

Parameter	Value	Unit	Description
$E_{\|\|}^f$	294	[GPa]	Longitudinal modulus fibre
$E_{\perp}^f$	14	[GPa]	Transverse modulus fibre
$G_{\|\|}^f$	8.78	[GPa]	Shear modulus LT
$\nu_{\|\|}^f$, $\nu_{\perp}^f$	0.2,0.2	[-]	Poissin's ratio fibre LT and TT
E^e	0.535	[GPa]	Young's modulus SBE
ν^e	0.38	[-]	Poisson's ration SBE
κ^e	$2 \cdot 10^{-2}$	[S/m]	Ion conductivity SBE
κ^f	$6.9 \cdot 10^4$	[S/m]	Electric conductivity carbon fibre
D_{Li}^e	$1.57 \cdot 10^{-13}$	$[m^2/s]$	Diffusion coefficient of Li^+ liquid phase of SBE
$c_{Li,max}^f$	25678	$[mol/m^3]$	Maximum Li-concentration fibre
$c_{Li,ini}^e$	1000	$[mol/m^3]$	Initial Li-concentration SBE
$c_{Li,ref}^e$	1	$[mol/m^3]$	Reference Li-concentration SBE
α_c, α_α	0.5	[-]	Anodic and cathodic transfer coefficients (Neg/Pos)
t_+	0.293	[-]	Transport number electrolyte
p_e	0.38	[-]	Porosity SBE
r_f	2.5	$[\mu m]$	Radius of carbon fibre
t_{neg}	25	$[\mu/layer]$	Thickness of negative electrode
t_{sep}	25	$[\mu m]$	Thickness of the separator
ρ_f	1850	$[kg/m^3]$	Density of carbon fibre
ρ_e	1100	$[kg/m^3]$	Density of SBE

Table A.1: Model parameters for the structural battery.